Article

Dual-site Controlled and Lysosome-targeted ICT-PET-FRET Fluorescent Probe for Monitoring pH Changes in Living Cells

Baoli Dong, Xuezhen Song, Chao Wang, Xiuqi Kong, Yonghe Tang, and Weiying Lin

Anal. Chem., **Just Accepted Manuscript** • DOI: 10.1021/acs.analchem.6b00422 • Publication Date (Web): 08 Mar 2016

Dual-site Controlled and Lysosome-targeted ICT-PET-FRET Fluorescent Probe for Monitoring pH Changes in Living Cells

Baoli Dong, Xuezhen Song, Chao Wang, Xiuqi Kong, Yonghe Tang, and Weiying Lin*

Institute of Fluorescent Probes for Biological Imaging, School of Chemistry and Chemical Engineering, School of Biological Science, University of Jinan, Jinan, Shandong 250022, P. R. China. Fax: (+) 86-531-82769031, E-mail: weiyinglin2013@163.com

ABSTRACT: Acidic pH is a critical physiological factor for controlling the activities and functions of lysosome. Herein, we report a novel dual-site controlled and lysosome-targeted ICT-PET-FRET fluorescent probe (CN-pH), which was essentially the combination of a turn-on pH probe (CN-1) and a turn-off pH probe (CN-2) by a non-conjugated linker. Coumarin and naphthalimide fluorophores were selected as donor and acceptor to construct FRET platform. Hydroxyl group and morpholine were simultaneously employed as the two pH sensing sites and controlled the fluorescence of coumarin and naphthalimide units by ICT and PET, respectively. The sensing mechanism of CN-pH to pH was essentially an integration of ICT, PET and FRET processes. Meanwhile, the morpholine also can serve as a lysosome-targeted group. Combing the two data analysis approaches of the ratios of the two emission intensities (R) and the reverse ratio R' (R'=1/R), the fluorescent ratio of CN-pH can show proportional relationship to pH values in a very broad range from pH 4.0 to 8.0 with high sensitivity. The probe has been successfully applied for the fluorescence imaging of the lysosomal pH values, as well as ratiometrically visualizing chloroquine-stimulated changes of intracellular pH in living cells. These features demonstrate the probe can afford practical application in biological systems.

■ INTRODUCTION

Intracellular pH is a critical physiological factor that relates closely with many biological processes including cellular apoptosis, proliferation and enzymatic activity.[1-3] As an important organelle for nearly all eukaryotic cells, lysosome plays important roles in cellular apoptosis, immunologic defence, intracellular digestion and specialized secretory functions.[4-6] An acidic environment with pH in the range of 4.5-5.5 could facilitate activating the functions of the acidic hydrolases, cathepsins, nucleases, lipases and other enzymes in lysosome.[7-9] By contrast, abnormal lysosomal pH value could give rise to dysfunctions, which are closely related to many diseases including cancer, shock and rheumatoid arthritis.[10-13] Thus, to precaution and diagnosis of these diseases, it is of great important to real-timely and precisely monitor the pH values of lysosome in living system.

Fluorescence imaging is a great powerful approach for monitoring cellular pH because of its numerous advantages, such as highly sensitivity, imperial spatiotemporal resolution, convenient operation, nondestructive test and real-time detection.[14-19] Fluorescence intensity-based probes are the pretty common probes, and tend to be disturbed by experimental conditions including probe environment and excitation intensity. By comparison, ratiometric fluorescent probe, the other important class of fluorescent probes, could alleviate above-mentioned problems by outputting ratiometric signal of the fluorescence intensities at two emissions bands instead of single emission intensity.[20-21] That is, the ratiometric probes can enable the accurate detection of pH values in a quantitative manner. So far, some ratiometric fluorescent probes that used for imaging lysosomal pH values have been developed.[22-30] However, these probes usually have obvious limitation in the sensitivity and sensing range of pH values, because the fluctuation of the lysosomal pH values is very small (generally less than 2.0). For example, the variation amplitudes of the ratiometric values for the reported ratiometric pH probes are usually less than 5 times in the lysosomal lumen pH 4.0-6.0. Thus, there is a great need in designing ratiometric probes with high sensitivity and broad sensing range of pH for monitoring lysosomal pH values.

Fluorescence resonance energy transfer (FRET) has been commonly exploited for the design of ratiometric fluorescent probes relative to other sensing mechanisms including intramolecular charge transfer (ICT) and photo-induced electron transfer (PET), because of its advantages in the high flexibility of the design of FRET-based probes and the wide choices of fluorophores. [31-36] Currently, there are some FRET-based fluorescent probes for monitoring cellular pH values have been developed.[28, 30, 37-40] However, these probes can be regarded as

Scheme 1. Design strategies for the FRTE-based fluorescent probes

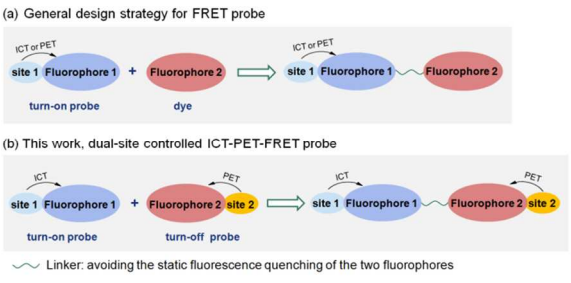

the combination of a turn-on pH probe and a dye, and generally employ only one pH sensing site to provide the single-site-dependent ratiometric fluorescence signal output by two sensing mechanism such as ICT-FRET, PET-FRET (Scheme 1a). Like FRET, ICT and PET are also the conventional sensing mechanisms for developing fluorescent pH probes. [41-43] The fluorescent probes that control fluorescence by multi-mechanism for generating changes in the emission wavelengths can tend to provide diversiform fluorescent signals or amplify the responding signals, which is beneficial for improving their sensitivity.[44-50] Thus, the development of highly sensitive fluorescent probe with multi-mechanism for monitoring lysosomal pH is still in demand.

In this work, we present a novel design strategy for developing lysosome-targeted ICT-PET-FRET fluorescent pH probe, which can be regarded as the combination of a turn-on pH probe and a turn-off pH probe by a non-conjugated linker (Scheme 1b). Two pH sites were employed simultaneously to control the optical properties of the two fluorophores by ICT and PET, respectively. Meanwhile, the FRET process exists between the two fluorophores. The pH probe based on this novel design strategy possesses highly sensitivity and a very broad pH detection range, and has been successfully applied for monitoring lysosomal pH changes in living cells.

■ EXPERIMENTAL SECTION

Materials and Instruments. Unless otherwise stated, all reagents were purchased from commercial suppliers and used without further purification. Twice-distilled water was used in all the experiments. TLC analysis was performed on silica gel plates and column chromatography was conducted over silica gel (mesh 200-300, Qingdao Ocean Chemicals). High-resolution electronspray mass spectra (HRMS) were obtained from Bruker APEX IV-FTMS 7.0T mass spectrometer. ^{1}H and ^{13}C NMR spectra were recorded on AVANCE III 400 MHz Digital NMR Spectrometer, using tetramethylsilane (TMS) as internal reference respectively. The pH measurements were carried out on a Mettler-Toledo Delta 320 pH meter. UV-Vis absorption spectra were measured on a Shimadzu UV-2600 spectrophotometer. Fluorescence spectra were recorded with a HITACHI F4600 fluorescence spectrophotometer. PMT Voltage was set at 400V or 700V for the fluorescence spectra. Data were expressed as mean standard deviation (SD) of three separate measurements.

Theoretical Calculations. The energy levels of HOMO and LUMO were determined by the density functional theory (DFT) and time-dependent density functional theory (TD-DFT) calculations using the Gaussian 09 software. The exchange-correlation functional of B3LYP with Becke's three parameter form was adopted and the basis set of 6-31G(d) was used in the calculations.

Cell Culture and Fluorescence Imaging. HeLa cells were cultured in modified Eagle's medium supplemented with 10% calf bovine serum in an atmosphere of 5% CO_2 and 95% air at 37 °C. Then cells were seeded into 35 mm glass-bottom culture dishes and cultured for 24h. For imaging at various pH, the cells were incubated with 5 μM CN-pH for 10 min at 37 °C, then the media was replaced with PBS buffer at various pH. The cells were sequentially incubated with the PBS buffer, 10.0 μM nigericin and 5.0 μM monensin for another 30 min, and then imaged using a Nikon A1R MP+ confocal microscope. For imaging pH changes stimulated by chloroquine, HeLa cells stained with 5 μM CN-pH for 20 min at 37 °C were washed three times with PBS buffer, and then 100 μM or 200 μM chloroquine was added to stimulate cellular pH change. Cell images were obtained using a Nikon A1R MP+ confocal microscope.

■ RESULTS AND DISCUSSION

Design Strategy of the Lysosome-targeted and ICT-PET-FRET pH Probe. The general design strategy for FRET probe allows the connection of a dye to a turn-on probe by a non-conjugated linker, and usually employs only one sensing site (Scheme 1a). Our design strategy features a FRET probe employing two sensing sites simultaneously to control the fluorescence of the two fluorophores by ICT and PET, respectively (Scheme 1b). That is, the sensing mechanism of the probe was essentially an integration of ICT, PET and FRET processes. More importantly, the novel probe can be regarded as the combination of a turn-on probe and a turn-off probe by a non-conjugated linker, which is beneficial for enhancing the range of their fluorescence intensity ratio logically.

Based on this novel design strategy and our previous studies on the FRET probes.[30, 37] we constructed a novel dual-site controlled and lysosome-targeted ICT-PET-FRET probe, CN-pH, which was essentially the combination of the probes CN-1 and CN-2 by a non-conjugated linker (Figure 1). In the probe, coumarin and naphthalimide fluorophores were selected to constructed FRET platform for the two main reasons. Firstly, the two fluorophores have significant advantages in optical properties, such as excellent photostability, high molar absorption coefficient and high fluorescence quantum yield. Secondly, due to the high overlap between the fluorescence of coumarin unit (donor) and the absorption of naphthalimide unit (acceptor), as well as the suitable distance (14.11 Å) between the two fluorophores calculated by Gaussian 09 software, the coumarin-naphthalimide platform could possess remarkable FRET efficiency. Hydroxyl and morpholine were employed as the two pH sensing sites and combined with coumarin and naphthalimide units, respectively. With the variation of the pH from acidity to alkalinity, the probe CN-1 exhibits turn-on fluorescence for the enhancement of the ICT efficiency, while the probe CN-2 exhibits turn-off fluorescence by the PET process. In addition, the morpholine can also be served as lysosome-targeted group. Figure 1 shows the synthesis routes of CN-pH, as well as CN-1 and CN-2 which can serve as the building blocks for CN-pH chemically. The structures of the compounds were determined by HRMS, ^{1}H and ^{13}C NMR spectra (Supporting Information).

pH-dependent Photoproperties of CN-1 and CN-2. Initially, we determined the pH-dependent photoproperties of CN-1 and CN-2 in Britton-Robinson (B-F) buffers. Under acidic condition (pH = 3.5), CN-1 had an absorption maximum at 345 nm with molar absorption coefficient (ε) of 2.96×10^4 $mol^{-1}.cm^{-1}$ (Figure S1). With the pH changing from 3.5 to 9.5, the absorption peaks of CN-1 located in the range of 320-370 nm exhibited obvious decrease of absorbance. When the pH exceeded 5.5, CN-1 showed new absorption bands located at 400 nm. At pH 3.5-9.5, CN-2 showed almost same absorbance located at about 430 nm with ε of about 2.02×10^4 $mol^{-1}.cm^{-1}$ in the visible region. When excited, CN-1 showed emissions at 454 nm and CN-2 showed emissions at 530 nm (Figure S2). As shown in Figure 2a, the overlap between the absorption spectra of CN-2 and the fluorescence spectra of CN-1

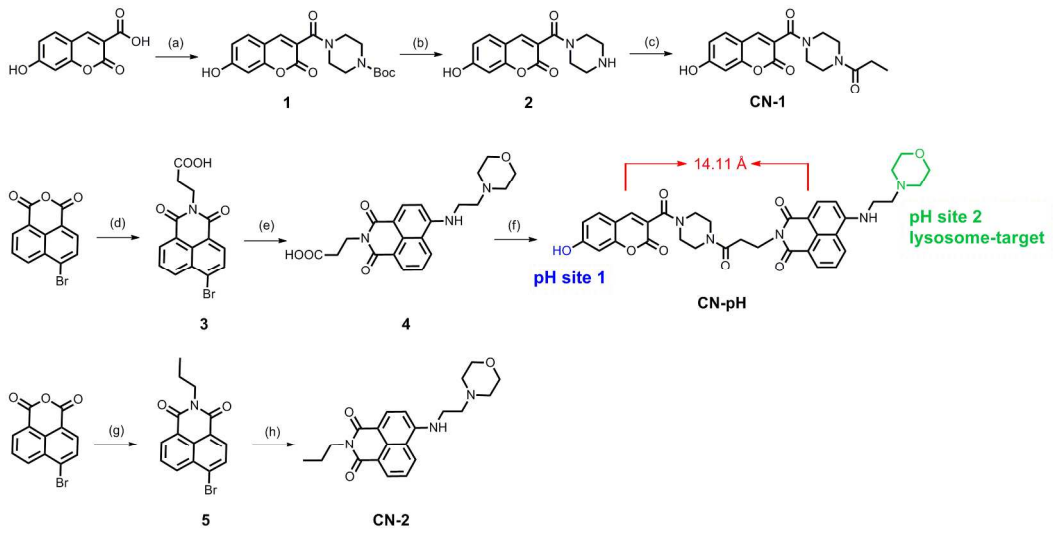

Figure 1. Synthesis routes of CN-1, CN-pH and CN-2. (a) *t*-butyl piperazine-1-carboxylate, EDCl, HOBt, DIEA, DMF, rt, 12 h; (b) CF_3COOH, CH_2Cl_2, 2 h; (c) propionic acid, EDCl, HOBt, DIEA, DMF, rt, 12 h; (d) 3-aminopropanoic acid, ethanol, reflux, 3 h; (e) 2-morpholinoethanamine, $Pd(OAc)_2$, BINAP, DMSO, Cs_2CO_3, 80 °C, 8 h; (f) compound **2**, EDCl, HOBt, DIEA, DMF, rt, 12 h; (g) propan-1-amine, ethanol, reflux, 3 h; (h) 2-morpholinoethanamine, $Pd(OAc)_2$, BINAP, DMSO, Cs_2CO_3, 80°C, 8 h.

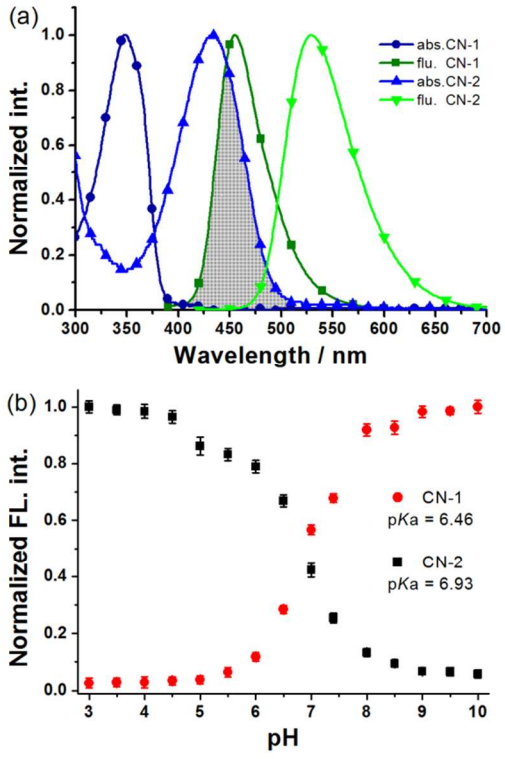

Figure 2. (a) Normalized absorption spectra (abs.) and fluorescence spectra (flu.) of 5 μM CN-1 and CN-2 at pH 5.0 in B-F buffers (5% MeOH). The gray area represented the overlap between the fluorescence spectrum of CN-1 and the absorption spectrum of CN-2. (b) Normalized fluorescence intensity of 5 μM CN-1 (λ_{em} = 454 nm) and CN-2 (λ_{em} = 530 nm) at various pH in B-F buffers (5% MeOH). Fluorescence spectra for CN-1, λ_{ex} = 380 nm; CN-2, λ_{ex} = 410 nm.

was significant and beneficial for the FRET from the excitation state of CN-1 to the ground state of CN-2. More importantly, CN-1 showed turn-on fluorescence with the pH changing from 3.0 to 10.0, while CN-2 showed turn-off fluorescence (Figure 2b). In addition, the p*K*a values of CN-1 and CN-2 were calculated to 6.46 and 6.93 using the Henderson-Hasselbalch equation. Therefore, the probes CN-1 and CN-2 could probably be combined into a dual-site controlled pH probe with high sensitivity and broad sensing range of pH.

Subsequently, the sensing mechanisms of CN-1 and CN-2 to pH were explored. When pH exceeds 5.5, the hydroxyl group of CN-1 can ionize a proton to generate negative oxygen ion, consisting with the new absorption located at 400 nm at pH 5.5-9.5 (figure S1). Because the negative oxygen ion possesses stronger electron-donating ability than hydroxyl, the ionization of hydroxyl is essentially beneficial for enhancing the ICT efficiency. Thus, CN-1 can show obvious turn-on fluorescence with the increase of pH values. For CN-2, the Gaussian calculations showed that the HOMO energy of 4-ethylmorpholine (-5.40 eV) is larger than the HOMO energy of 4-aminonaphthalimide fluorophore (-5.74 eV), and smaller than its LUMO energy (-2.18 eV). It suggests that the reductive PET (a-PET) from morpholine to fluorophore occurs when the fluorophore is excited, and quenches the fluorescence of 4-aminonaphthalimide fluorophore (Figure S3). At acidic condition, the protonation of amino at morpholine blocks the a-PET process and enables the naphthalimide fluorophore to emit fluorescence. Thus, CN-2 can show obvious turn-off fluorescence with the increase of pH values. Taken together, the hydroxyl group and morpholine can be served as the response sites of CN-1 and CN-2 to pH, and control the fluorescence of coumarin and naphthalimide fluorophores by ICT and PET mechanisms, respectively.

Optical Response of CN-pH to pH. UV-Vis spectra of CN-pH at various pH values are shown in Figure 3a. Compared with the above-mentioned absorption spectra of CN-1

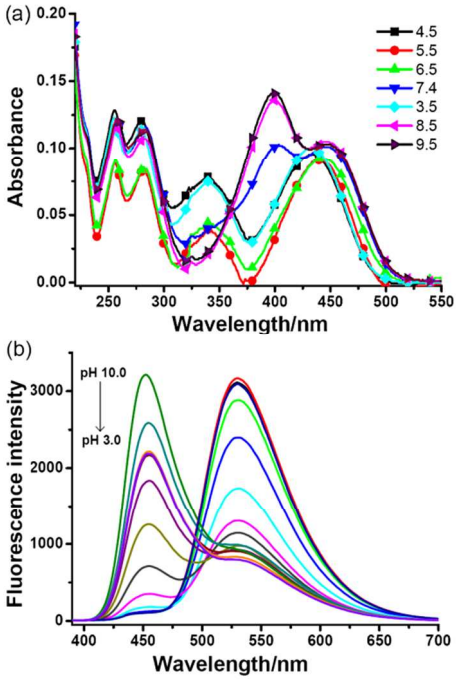

Figure 3. Absorption spectra (a) and fluorescence spectra (b, λ_{ex} = 380 nm) of 5 μM CN-pH in B-F buffers (5% MeOH) at various pH values.

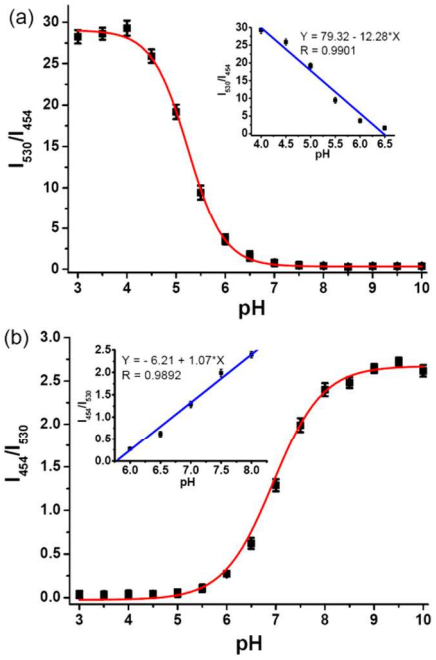

Figure 4. Fluorescence intensity ratios I_{530}/I_{454} (a) and I_{454}/I_{530} (b) of 5 μM CN-pH in B-F buffers (5% MeOH) at various pH. Insets were the linear plots of fluorescence intensity ratio to pH. λ_{ex} = 380 nm.

and CN-2, the absorption bands of CN-pH peaked at about 345 nm and 400 nm arose from coumarin moiety, while the absorption bands located at 257 nm, 280 nm and 430 nm can be ascribed to naphthalimide unit. That is, the absorption of CN-pH at various pH values was thoroughly superposed by the absorption of CN-1 and CN-2, indicating that there is no interaction (mainly π-π interaction) between the coumarin and naphthalimide fluorophores in CN-pH molecule.

We then explored the fluorescence response of CN-pH to pH by determining the fluorescence spectra of CN-pH at various pH in B-F buffers. At acidic condition (pH = 3.0), CN-pH showed weak blue emission at 454 nm and strong green emission at 530 nm (Figure 3b). When the pH changed from 3.0 to 10.0, the blue emission increased and the green emission decreased gradually. The ratios of fluorescence intensities *R* (I_{530}/I_{454}) showed a significant change (up to 58-fold) from 0.5 at pH 7.4 to 29.3 at pH 4.0, overlapping the lysosomal pH (4.5-5.5) and normal physiological pH range (6.2-7.4) and indicating CN-pH is suitable for assessing acidic media in lysosome. At pH 4.0-6.5, the ratio value *R* (I_{530}/I_{454}) was linearly proportional to pH (Figure 4a). When the data were treated with the reverse ratio of R' (R' = 1/R = I_{454}/I_{530}), R' can show an obvious enhancement (up to 15-fold) and linearly proportional to pH 6.0-8.0 (Figure 4b). Namely, combing the two data analysis approaches of R and R', the fluorescent ratiometric values of CN-pH can show proportional relationship to pH in a very broad range from pH 4.0 to pH 8.0, which was obviously broader than that of the reported fluorescent pH probe. Therefore, CN-pH can be used for the precise pH measurement from pH 4.0 to pH 8.0 in a ratiometric manner, and has potential capability of sensing lysosomal pH changes in living system.

The fluorescence response mechanism of CN-pH to pH was further investigated on the basic of the pH-dependent fluorescence spectra of CN-1, CN-2, as well as the mixture of CN-1, CN-2 in B-F buffers. Obviously, the blue emission located at 454 nm of CN-pH arose from coumarin unit and the green emission located at 530 nm can be ascribed to naphthalimide unit. Excited at 380 nm, the mixture of CN-1, CN-2 in B-F buffers showed mainly blue emission arose from coumarin unit because the UV light at 380 nm was primarily absorbed by coumarin unit instead of naphthalimide unit (Figure S4 and S5). By contrast, CN-pH can show relative strong green emission arose from naphthalimide unit when excited at 380 nm, indicating the FRET process from coumarin to naphthalimide unit substantially occurred (Figure 3b). According to the theoretical calculations using MarvinSketch software, three main forms of CN-pH existed at pH 3.0-10.0 due to the ionization of hydroxyl and the protonation of amino group at morpholine (Figure 5 and Figure S6). In form **a**, the inhibition of the a-PET process enabled the naphthalimide fluorophore to emit fluorescence, and the FRET process from coumarin to naphthalimide occurred simultaneously. The a-PET process can happen in forms **b** and **c**, while the ICT proceeded with the ionization of hydroxyl in from **a**. That is, forms **a, b** and **c** can emit strong green fluorescence, weak blue fluorescence and strong blue fluorescence, which consisted well with the fluorescence photographs of CN-pH at pH 4.5, 6.5 and 6.5 (Figure 5). Therefore, the hydroxyl and morpholine can be served as the two pH response sites of CN-pH to synergistically control its fluorescence properties at various pH, and the response mechanism of CN-pH to pH was essentially an integration of ICT, PET and FRET processes.

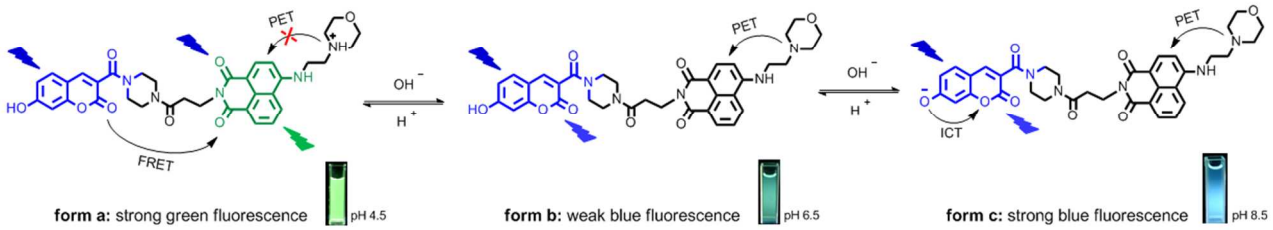

Figure 5. Proposed sensing mechanism and the fluorescence photographs of 5 μM CN-pH at pH 4.5, 6.5 and 8.5 under 365 nm.

To evaluate the specificity of CN-pH, the fluorescence spectra of CN-pH were determined coexisting with biologically relevant species at various pH. We selected a series of ions and small biomolecules that commonly exist in living systems as potential interfering substances, including Ca^{2+}, Mg^{2+}, Cu^{2+}, H_2O_2, Cys, GSH, H_2S, SO_2 and NO. Taking into consideration of the lysosomal pH at 4.5-5.5 and normal physiological pH at about 7.4, we chose three test systems at pH 4.5, 5.5 and 7.4. The ratios (I_{530}/I_{454}) had no significant changes after adding the various ions or small biomolecules at pH 4.5, 5.5 and 7.4 (Figure S7). Therefore, CN-pH can potentially monitor the lysosomal pH changes in living system.

The time-dependent ratios (I_{530}/I_{454}) of CN-pH were also determined at pH 4.5, 5.5 and 7.4. As shown in Figure S8, when CN-pH was added into the solutions with difference pH, the ratios (I_{530}/I_{454}) reached equilibrium in a short time (less than 1min). In addition, we also studied the reversibility of CN-pH in solutions at pH 5.5 and 7.4. The results suggested that the process can be reversibly performed for at least six cycles (Figure S9). Therefore, CN-pH was can show real-time and reversible fluorescence response to pH.

Fluorescence Imaging in Living Cells. Encouraged by the desirable pH-dependent spectral properties of CN-pH, we then examined the biological applications of the probe for monitoring pH changes in living cells. Initially, colocalization experiments were performed in HeLa cells using CN-pH and a known lysosome-specific fluorescent probe, LysoTracker Red®, to determine the presumed lysosome-target property of the probe. The HeLa cells were incubated with CN-pH (5.0 μM) for 10 min at 37 °C, and then medium was replaced with fresh medium containing LysoTracker Red® (1.0 μM) and the cells were incubated for another 10 min. As shown in Figure 6, the cells showed blue and green fluorescence from CN-pH, and red fluorescence from LysoTracker Red® simultaneously. Because CN-pH can emit stronger green fluorescence relative to blue fluorescence at pH 7.4, the overlap between the green and red fluorescence images was determined to evaluate the lysosome-targeted property of the probe. The Pearson's correlation coefficient between green and red fluorescence images was calculated to 0. 82, confirming the probe distributed mainly in the lysosomes and possessed lysosome-targeted property. In addition, MTT assay indicated that CN-pH has no marked toxicity to HeLa cells below 10μM (Figure S10).

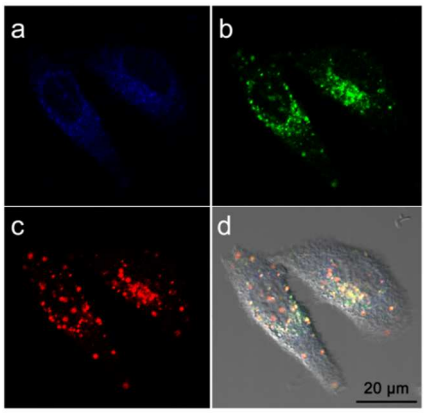

Figure 6. Colocalization experiments of CN-pH and LysoTracker Red® in HeLa cells. (a) blue fluorescence images for CN-pH (425-475 nm) with excitation at 405 nm; (b) green fluorescence images for CN-pH (500-550 nm) with excitation at 488 nm; (c) red fluorescence images for LysoTracker Red® (570-620 nm) with excitation at 561 nm; (d) overlay of (a), (b) and (c).

We then utilize CN-pH to estimate cellular pH values in a ratiometric manner. The cells were incubated with 5.0 μM CN-pH for 10 min at 37 °C, then the media was replaced with buffers at pH 4.0, 5.0, 6.0, 7.0 or 8.0. The cells were sequentially incubated with the buffer, 10.0 μM nigericin and 5.0 μM monensin for another 30 min.[23, 28] As shown in Figure 7a, the blue fluorescence showed obvious enhancement gradually with pH varing from 4.0 to 8.0, while the green fluorescence was was decreased gradually. Meanwhile, when quantified using Nikon NIS Element software, the blue and green fluorescence intensity showed turu-on and turn-off behaviors, respectively (Figure 7b). The ratio of R (I_{green}/I_{blue}) also exhibited significant changes from pH 4.0 (R = 3.48 ± 0.21) to 8.0 (R = 0.88 ± 0.11), consisting with the above-mentioned response of CN-pH to pH in B-F buffers. The statistical significance results showed that the quantified ratio (I_{green}/I_{blue}) at pH 4.0 exhibited an obvious difference from that at pH 6.0 (R = 2.28 ± 0.20) with $p < 0.05$, and a significant difference from that at pH 7.0 (R = 1.17 ± 0.16) and 8.0 with $p < 0.01$ (Figure 7c). Taken together, CN-pH can show desirable sensitivity in monitoring cellular pH values. To the best of our knowledge, CN-pH is the first pH probe based on ICT-PET-FRET mechanism that can be used in the fluorescence imaging of cellular pH.

Subsequently, CN-pH was employed to ratiometrically visualize the chloroquine-stimulated intracellular pH changes in living HeLa cells. Chloroquine is a lysosomotropic agent that can inhibit autophagy and protein degradation by raising the lysosomal pH.[51] Before the treatment of chloroquine, the cells showed fluorescence in both blue and green channels with the fluorescence intensity ratio (I_{green}/I_{blue}) of 2.50 ± 0.13

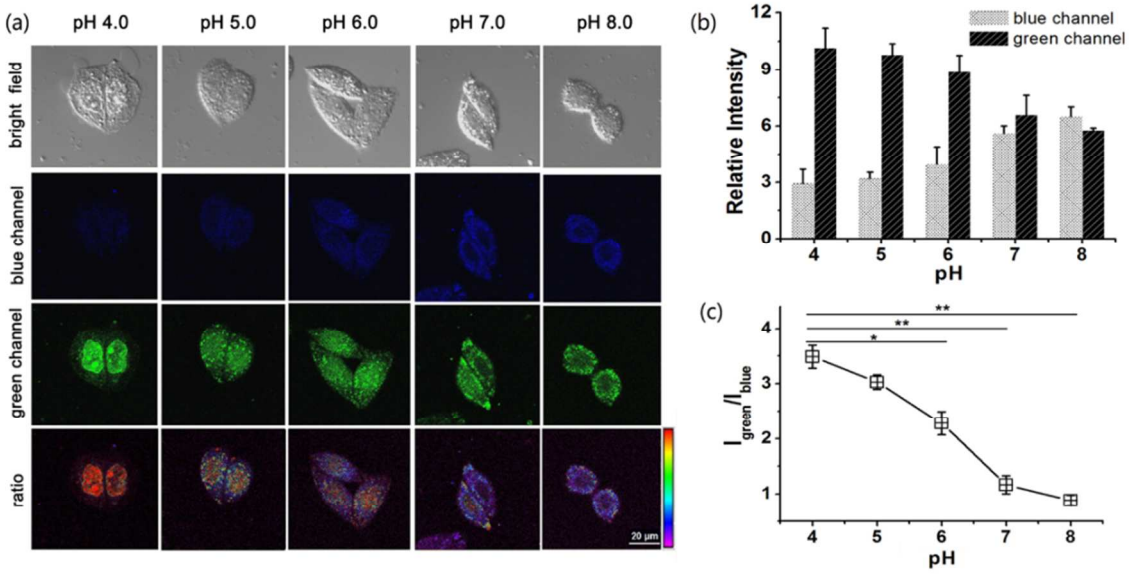

Figure 7. (a) Fluorescence images for 5 μM CN-pH in HeLa cells at various pH. Blue channel, emission at 425-475 nm with excitation at 405 nm. Green channel, emission at 500-550 nm with excitation at 488 nm. Ratio images represent the ratio of fluorescence intensity between green channel and blue channel (I_{green}/I_{blue}). (b) Quantified relative fluorescence intensity at various pH was analyzed using Nikon NIS Element software and presented as mean ± s.d with, n = 3. (c) Ratio of I_{green}/I_{blue} at various pH obtained from (b). Statistical analyses were performed with Student's *t*-test (n = 3). * $P < 0.05$, *$P < 0.01$ and error bars are ± s.d.

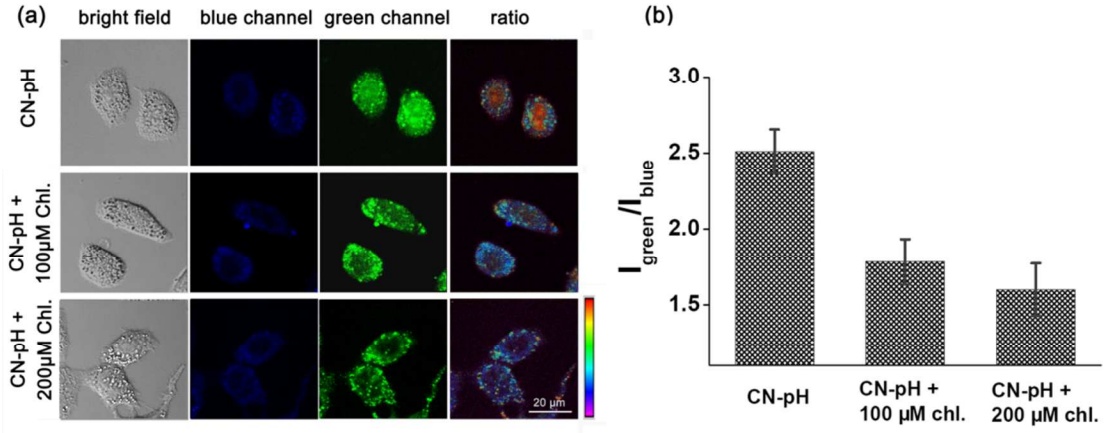

Figure 8. (a) Fluorescence imaging of lysosomal pH changes in HeLa cells stimulated with 100 μM and 200 μM chloroquine. Blue channel, emission at 425-475 nm with excitation at 405 nm. Green channel, emission at 500-550 nm with excitation at 488 nm. (b) Quantified relative fluorescence ratio of I_{green}/I_{blue} of images analyzed using Nikon NIS Element software and presented as mean ± s.d, n = 3.

(Figure 8a and 8b). According to the above-mentioned ratios (I_{green}/I_{blue}) of CN-pH in living HeLa cells (Figure 7c), the lysosomal pH value of the cells untreated with chloroquine was calculated to be about 5.5, which is in the normal lysosomal pH range of 4.5 - 5.5. After the treatment with 100 μM chloroquine for 20 min, the cells exhibited slightly increased blue and decreased green fluorescence with the fluorescence intensity ratio (I_{green}/I_{blue}) of 1.78 ± 0.15 corresponding to the pH of about 6.4. Under the same conditions, when the cells were treated with higher concentration of chloroquine (200 μM), the cells can show relative obvious decreased green fluorescence with the fluorescence intensity ratio (I_{green}/I_{blue}) of 1.50 ± 0.17 corresponding to the pH of about 6.6. These results indicate that CN-pH can be applied for monitoring the chloroquine-induced lysosomal pH changes within a small range.

■ CONCLUSIONS

In summary, we have developed a novel dual-site controlled and lysosome-targeted ICT-PET-FRET fluorescent probe (CN-pH) for monitoring lysosomal pH values in living cells. The probe adopted coumarin and naphthalimide fluorophores as donor and acceptor to construct FRET platform, as well as employed hydroxyl and morpholine simultaneously as the two

pH sensing sites to control the fluorescence of coumarin and naphthalimide by ICT and PET, respectively. With the pH varying from 3.0 to 10.0, the coumarin unit showed blue turn-on fluorescence at 454 nm while the naphthalimide unit exhibited green turn-off fluorescence at 530 nm. Under the synergistic effects of ICT, PET and FRET, CN-pH can show excellent response to pH with high sensitivity. Combing the two data analysis approaches of R and the reverse ratio R', the fluorescent ratios of CN-pH can show proportional relationship to pH values in a broad range from pH 4.0 to pH 8.0, which obviously exceeded that of the developed FRET-based pH probe. CN-pH had no marked toxicity to living cells and possessed desirable lysosome-targeted property. CN-pH has been successfully applied for the fluorescence imaging of the lysosomal pH values, as well as ratiometrically visualizing chloroquine-stimulated changes of intracellular pH in living cells. These features demonstrate the probe can afford practical application for monitoring pH changes in pathogenic cells.

■ ASSOCIATED CONTENT

Supporting Information

The Supporting Information is available free of charge on the ACS Publications website.

Synthesis of the probes, absorption and fluorescence spectra, theoretical calculations, ^{1}H and ^{13}C NMR spectra. (PDF)

AUTHOR INFORMATION

Corresponding Author

Fax: (+) 86-531-82769031, E-mail: weiyinglin2013@163.com

Notes

The authors declare no competing financial interest.

ACKNOWLEDGMENT

This work was financially supported by NSFC (21172063, 21472067), Doctoral Fund of University of Jinan (160082104), Shandong Provincial Natural Science Foundation (ZR2014BP002), and the startup fund of University of Jinan. We also thank the Special Foundation for Taishan Scholar Professorship of Shandong Province (TS 201511041).

REFERENCES

(1) Appelqvist, H.; Waster, P.; Kagedal, K.; Ollonger, K. *J. Mol. Cell Biol.* **2013**, *5*, 214-226.

(2) Luzio, J.P.; Pryor, P.R.; Bright, N.A. *Nat. Rev. Mol. Cell Biol.* **2007**, *8*, 622-632.

(3) Bainton, D.F. *Cell. Biol.* **1981**, *91*, 66-76.

(4) Saftig, P.; Klumperman, J. *Nat. Rev. Mol. Cell Biol.* **2009,** *10*, 623-635.

(5) Watts, C. *Biochim. Biophys. Acta.* **2012,** *1824*, 14-21.

(6) Zhao, H. *Traffic*. **2012**, *13*, 1307-1314.

(7) Casey, J. R.; Grinstein, S.; Orlowski, J. *Nat. Rev. Mol. Cell Biol.* **2010**, *11*, 50-61.

(8) Mellman, I.; Fuchs, R.; Helenius, A. *Annu. Rev. Biochem*. **1986,** *55*, 663-700.

(9) Martinez-Zaguilan, R.; Seftor, E. A. *Clin. Exp. Metastasis*. **1996**, *14*, 176-186.

(10) Schindler, M.; Grabski, S.; Hoff, E.; Simon, S.M. *Biochemistry*. **1996**, *35*, 2811-2817.

(11) Ellis, D.; Thomas, R. C. *Nature*. **1976**, *262,* 224-225.

(12) Zhang, R. G.; Kelen, S. G.; Lamanna, J. C. *J. Appl. Phys*.**1990**, *68*, 1101-1106.

(13) Hesse, S. J. A.; Ruijter, G. J. G.; Dijkema, C.; Vissser, J. *J. Biotechnol*, **2000**, *77*, 5-15.

(14) Singha, S.; Kim, D.; Seo, H.; Cho, S.W.; Ahn, K. H. *Chem. Soc. Rev.*, **2015**, *44*, 4367-4399.

(15) Li, X. H.; Gao, X. H.; Shi, W.; Ma, H. M. *Chem. Rev.*, **2014**, *114*, 590-659.

(16) Liu, J.; Sun, Y. Q.; Huo, Y.Y.; Zhang, H. X.; Wang, L. F.; Zhang, P.; Song, D.; Shi, Y. W.; Guo, W. *J. Am. Chem. Soc.* **2014**, *136*, 574-577.

(17) Lv, H.M.; Yang, X.F.; Zhong, Y.G.; Guo, Y.; Li, Z.; Li, H. *Anal. Chem*. **2014**, *86*, 1800-1807.

(18) Carter, K. P.; Young, A. M.; Palmer, A. E. *Chem. Rev.*, **2014**, *114*, 4564-4601.

(19) Li, L.; Li, P.; Fang, J.; Li, Q.L.; Xiao, H.B.; Zhou, H.; Tang, B. *Anal. Chem.* **2015**, *87*, 6057-6063.

(20) Kikuchi, K.; Takakusa, H.; Nagano, T. *Trends Anal. Chem*. **2004,** *23*, 407-415.

(21) Yuan, L.; Lin, W.Y.; Zheng, K.B.; Zhu, S.S. *Accouts Chem. Res.* **2013**, *46*, 1462–1473.

(22) Wu, S.; Li, Z.; Han, J.; Han, S. *Chem. Commun*., **2011**, *47*, 11276-11278.

(23) Kim, H.; Heo, C.; Kim, H. *J. Am. Chem. Soc.* **2013***, 135,* 17969−17977.

(24) Fan, J.; Lin, C.; Li, H.; Zhan, P.; Wang, J.; Cui, S.; Hu, M.; Cheng, G.; Peng, X. *Dyes Pigments,* **2013***, 99,* 620-626

(25) Li, G.; Zhu, D.; Xue, L.; Jiang, H. *Org. Lett*., **2013**, *15*, 5020-5023.

(26) Hu, J.; Wu, F.; Feng,S.; Xu, J.; Xu, Z.; Chen, Y.; Tang, T.; Weng, X.; Zhou, X. *Sens. Actuators B*, **2014**, *196*, 194-202.

(27) Chao, J.; Liu,Y.; Sun, J.; Fan, L.; Zhang,Y.; Tong, H.; Li, Z. *Sens. Actuators B*, **2015**, *221*, 427-433.

(28) Zhang, X.; Zhang,T.; Shen, S.; Miao, J.; Zhao, B. *J. Mater. Chem. B,* **2015***, 3,* 3260-3266.

(29) Wang, Q.; Zhou, L.; Qiu, L.; Lu, D.; Wu, Y.; Zhang, X. *Analyst.* **2015***,140*, 5563-5569.

(30) Zhang, X.; Zhang, T.; Shen, S.; Miao, J.; Zhao, B. *RSC Adv.*, **2015**, *5*, 49115-49121.

(31) Demchenko, A.P. *J. Fluoresc*. **2010**, *20*, 1099-1128.

(32) Fan, J.L.; Hu, M.M.; Zhan, P.; Peng, X.J. *Chem. Soc. Rev.*, **2013**,*42*, 29-43.

(33) Prevo, B.; Peterman, E. J. G. *Chem. Soc. Rev.,* **2014***, 43,* 1144-1155.

(34) Hohng, S.; Lee, S.; Lee, J.; Jo, M. H. *Chem. Soc. Rev.*, **2014**, *43,* 1007-1013.

(35) Hohlbein, J.; Craggs, T. D.; Cordes, T. *Chem. Soc. Rev*., **2014**, *43*, 1156-1171.

(36) Srikun, D.; Miller, E. W.; Domaille, D. W. *J. Am. Chem. Soc*. **2008**, *130*, 4596-4597.

(37) Yuan, L.; Lin, W. Y.; Cao, Z. M.; Wang, J. L.; Chen, B. *Chem. Eur. J*, **2012**, *18*, 1247-1255.

(38) Lv, H.; Huang, S.; Zhao, B.; Miao, J. *Anal. Chim. Acta*. **2013**, *788*, 177-182.

(39) Reddy, U.; Anila, H. A.; Ali, F. Taye, N.; Chattopadhyay, S.; Das, A. *Org. Lett.*, **2015**, *17*, 5532-5535.

(40) Georgiev, N. I.; Bryaskova, R.; Tzoneva, R.; Ugrinova, I.; Detrembleur, C.; Miloshev, S.; Asiri, A. M.; Qusti, A.H.; Bojinov, V. B. *Bioorg. Med. Chem*. **2013**, *21*, 6292-6302.

(41) Lee, M. H.; Kim, J. S.; Sessler, J. L. *Chem. Soc. Rev*., **2015**, *44*, 4185-4191.

(42) Chen, X.Q.; Zhou, Y.; Peng, X. J.; Yoon, J. *Chem. Soc. Rev.*, **2010**, *39*, 2120-2135.
(43) Zhou, Y.; Zhang, J. F.; Yoon, J. *Chem. Rev.*, **2014**, *114,* 5511-5571.
(44) Wandell, R. J.; Younes, A. H.; Zhu, L. *New J. Chem.*, **2010**, *34*, 2176-2182.
(45) Georgie, N. I.; Asiri, A. M.; Qusti, A. H.; Alamry, K. A.; Bojinov, V. B. *Dyes Pigm.*, **2014**, *102*, 35-45.
(46) Georgiev, N. I.; Asiri, A. M.; Alamry, K. A.; Obaid, A.Y.; Bojinov, V. B. *J. Photochem. Photobiol. A,* **2014**, *277*, 62-74.
(47) Georgiev, N. I.; Sakr, A. R.; Bojinov, V. B. *Sensors Actuators B*, **2015**, *221*, 625-634.
(48) Georgiev, N. I.; Dimitrova, M. D.; Asiri, A. M.; Alamry, K. A.; Bojinov, V. B. *Dyes Pigments,* **2015**, *115*, 172-180.
(49) Alamry, K. A.; Georgiev, N.; El-Daly, S. A.; Taib, L. A.; Bojinov, V. B. *J. Lumin*. **2015**, *158*, 50-59.
(50) Alamry, K. A.; Georgiev, N. I.; El-Daly, S. A.; Taib, L. A.; Bojinov, V. B. *Spectrochim. Acta A,* **2015**, *135*,792-800.
(51) Gonzalez-Noriega, A.; Grubb, J. H.; Talkad, V.; Sly, W. S. *J. Cell Biol*. **1980**, *85,* 839-852.

for TOC only: